Title	AlGaN/GaN high electron mobility transistor heterostructures grown by ammonia and combined plasma-assisted ammonia molecular beam epitaxy
Authors	Alyamani, Ahmed;Lutsenko, Evgenii V.;Rzheutski, Mikalai V.;Zubialevich, Vitaly Z.;Vainilovich, Aliaksei G.;Svitsiankou, Illia E.;Shulenkova, Varvara A.;Yablonskii, Gennadii P.;Petrov, Stanislav I.;Alexeev, Alexey N.
Publication date	2019-04-29
Original Citation	Alyamani, A., Lutsenko, E. V., Rzheutski, M. V., Zubialevich, V. Z., Vainilovich, A. G., Svitsiankou, I. E., Shulenkova, V. A., Yablonskii, G. P., Petrov, S. I. and Alexeev, A. N. (2019) 'AlGaN/GaN high electron mobility transistor heterostructures grown by ammonia and combined plasma-assisted ammonia molecular beam epitaxy', Japanese Journal of Applied Physics, 58(SC), SC1010 (5pp). doi: 10.7567/1347-4065/ab06b4
Type of publication	Article (peer-reviewed)
Link to publisher's version	10.7567/1347-4065/ab06b4
Rights	© 2019, The Japan Society of Applied Physics. This Accepted Manuscript is available for reuse under a CC BY-NC-ND 3.0 licence after the 12 month embargo period provided that all the terms of the licence are adhered to. - https://creativecommons.org/licenses/by-nc-nd/3.0/
Download date	2023-05-05 08:49:09
Item downloaded from	http://hdl.handle.net/10468/8461

University College Cork, Ireland
Coláiste na hOllscoile Corcaigh

AlGaN/GaN HEMT heterostructures grown by NH_3 and combined PA-NH_3 MBE

Ahmed Alyamani[1]*, Evgenii V. Lutsenko[2], Mikalai V. Rzheutski[2], Vitaly Z. Zubialevich[3], Aliaksei G. Vainilovich[2], Illia E. Svitsiankou[2], Varvara A. Shulenkova[2], Gennadii P. Yablonskii[2], Stanislav I. Petrov[4], and Alexey N. Alexeev[4]

[1]*KACST, National Nanotechnology Center, PO BOX 6086, 11442 Riyadh, Saudi Arabia*

[2]*Institute of Physics of NAS of Belarus, 68 Nezalezhnasci Ave. 220072, Minsk, Belarus*

[3]*Tyndall National Institute, University College Cork, Lee Maltings, Dyke Parade, Cork, Ireland*

[4]*SemiTEq JSC, 27 Engels Ave. 194156, Saint-Petersburg, Russia*

*E-mail: ayamani@kacst.edu.sa

The structural properties and surface morphology of AlN epitaxial layers grown by ammonia (NH_3) and plasma-assisted (PA) molecular beam epitaxy (MBE) with varied growth condition (ammonia flow and substrate temperature) on (0001) sapphire were investigated. The lowest root-mean-square roughness of ~0.7 nm was achieved for the sample grown by ammonia-MBE at 1085°C and NH_3 flow of 100 standard cm^3/min. This sample demonstrated a terrace-monolayer step-like surface morphology as acquired by atomic force microscopy (AFM). Further, the optimal substrate temperature for growth of GaN and AlGaN layers was determined from analysis of GaN thermal decomposition rate. Based on the results, high electron mobility transistor (HEMT) heterostructures were grown by NH_3-MBE and combined MBE (initially PA-MBE for nucleation layer and then NH_3-MBE for the rest of structures) which demonstrated relatively good 2-dimensional electron gas (2DEG) properties. A slightly higher 2DEG mobility of ~2000 $cm^2/(V \cdot s)$ at a decent 2DEG density of ~$1.17 \cdot 10^{13}$ cm^{-2} was obtained for the combined MBE HEMT heterostructure.

1. Introduction

In the last two decades, gallium nitride (GaN) and related materials (AlGaN, AlN) have attracted much interest as a promising material system for high power and high frequency electronic devices. It is caused by a number of superior properties of these materials such as wide bandgap, high electric breakdown field, high-electron saturation velocity.[1-4] GaN-based high electron mobility transistors (HEMTs) are considered as main alternative to Si- and GaAs-based transistors in microwave and millimetre-wave applications (wireless communication systems, radar systems etc.) as well as in power conversion electronics.[5] Recently, a number of impressive achievements was demonstrated for GaN-based HEMTs, including a high drain current[6], high breakdown voltage[7] and a high operating frequency[8] combined with the ability to work in extreme conditions. For GaN HEMTs, 2-dimensional electron gas (2DEG) mobility and 2DEG density are the most critical characteristics defining their overall performance. Their current state of the art values are about ~2000 $cm^2/(V \cdot s)$ at no lower than 10^{13} cm^{-2}, respetively.[9-11] However, despite of the recent achievements, the GaN HEMT technology needs further improving. In the absence of the cheap native GaN substrates, heteroepitaxy of GaN on foreign substrates (Si, sapphire, or SiC) is the only viable alternative. The main problem of this route however is the lattice mismatch between GaN and the foreign substrates used. The heteroepitaxy on lattice mismatched substrates results in gradual building-up of mechanical stress during the growth which is partly released by plastic deformation via generation of misfit dislocations and in some cases even cracks. As the growth proceeds, some dislocation will merge or annihilate but many will thread through the 2DEG region until they end at the surface. Such treading dislocations act as electron scattering centres degrading the 2DEG mobility[12] and thus overall device performance.

While one of the most important problems of GaN-based power electronics is a development of reliable growth technology on Si substrates (because of their low cost and availability in the form of large diameter wafers), GaN epitaxy on sapphire is also an actual issue for some applications (sensors[13-15], low power high frequency devices etc.). Moreover, nitride epitaxy on sapphire substrates can be used for a preliminary technology optimisation because of its relatively low cost and fairly good quality.

In contrast to the commonly used in III-nitride epitaxy metalorganic chemical vapour deposition (MOCVD) and plasma-assisted (PA) molecular beam epitaxy (MBE) technologies, an ammonia (NH_3) MBE is less investigated despite the combination in it of

some benefits of both MOCVD and PA MBE (high growth temperature, high vacuum and ability of creation of sharp heterointerfaces). In this work, we report results on optimisation of MBE growth conditions of AlN nucleation and buffer layers on sapphire substrates for HEMT heterostructures.

2. Experimental methods

All the investigated epitaxial structures were grown in a STE3N MBE system (SemiTeq) on 2-inch (0001) sapphire substrates with a root-mean-square (RMS) roughness of less than 0.2 nm and a surface misorientation of about 0.2°. Both NH_3 and PA MBE were used during the experiment. Prior to the growth, the substrates were annealed at 1000°C for 30 min and nitridated for 10 min at 30 cm^3/min NH_3 flow and 850°C (all gas flow values in the paper are given for the standard state). Alternatively, the latter step was done in 3 cm^3/min of nitrogen plasma flow at 740°C. In addition to NH_3 and PA MBE, a combined MBE was used within a single epitaxy process. In this case, a PA MBE grown nucleation AlN layer was followed by NH_3 MBE growth of the rest structure in the same growth chamber. Other growth conditions details are described below. Quality of the AlN buffer layers was controlled by scanning electron microscope (SEM, Carl Zeiss Supra 40), atomic force microscope (AFM, Nanoflex Solar LS) and X-ray diffraction (XRD, PANalytical X'pert PRO) analysis. 2DEG mobility and density of HEMT heterostructures were measured by contactless Lehighton 1605B setup at different points on a wafer.

3. Results and discussion

3.1 Optimisation of ammonia-MBE growth of AlN layers

The nucleation and buffer layers growth is the most important step in epitaxy of III-nitride-based devices because defects in the early grown layers governs a quality of an active structure substantially.[16, 17] To determine optimal ammonia-MBE growth conditions of nucleation and buffer AlN layers, a series of 0.32 μm thick AlN epilayers were grown at different substrate temperatures varied from 800°C to 1190°C and NH_3 flows from 30 cm^3/min to 100 cm^3/min. The epitaxial processes were started with the growth of the AlN nucleation layer at very low rate (v_{gr} ~ 0.05 μm/hour) followed by its gradual increase to 0.2 μm/hour within the first 80 nm of AlN. The growth rate was controlled by varying of the Al-source temperature while NH_3 flow was kept constant. The very low growth rate starting was intended to provide better surface morphology and less dislocation density in the nucleation AlN layer.[18] The favourable effect of the lower growth rate was explained by

Chaumeton et al.,[18] and lays in reducing of initial nucleation density during the first monolayers growth leading to more pronounced 2-dimensional growth mode.

The effects of NH_3-MBE growth conditions are demonstrated by SEM images shown in Fig. 1 together with RMS surface roughness values σ obtained by AFM. It is seen from the figure, that a low substrate temperature $T \leq 1010$°C promotes a polycrystalline growth leading to formation of misoriented crystallites (no epitaxial relation with the substrate). The layers grown at higher temperatures demonstrate much better crystallinity. An increase of NH_3 flow from 50 cm^3/min to 100 cm^3/min at $T = 1085$°C results in formation of flat terraces having a width of up to 0.8 μm and demonstrating a step-flow growth mode (the terraces-like morphology was also observed by AFM). The minimal RMS surface roughness of ~0.7 nm was achieved for AlN layer grown at $T = 1085$°C and NH_3 flow of 100 cm^3/min. A further increase of substrate temperature leads to rise of RMS surface roughness because of formation of hexagonal prismatic-shaped hills on a layer surface. An origin of the hills is not clear now. Other authors ascribe similar defects to inversion domains.[19-21]

In order to reveal effect of NH_3-MBE growth conditions on structural properties of AlN, XRD rocking curves for the 002 and 101 reflections were measured which are sensitive to screw and edge dislocation densities correspondingly[22, 23]. In Fig. 2, the FWHM values for the reflections are plotted as a function of substrate temperature. For the both types of reflections, a clear tendency of decrease of FWHM when growth temperature rises from 800°C to 1085°C is observed. A further increase of the growth temperature doesn't change the FWHM substantially. The observed behaviour indicating decrease of dislocation density with growth temperature rise[24-26] is not surprising taking into account the fact that the growth temperature governs the adatom diffusion, which is responsible for the material quality. In our case, the lowest total dislocation density was determined for the AlN layers grown at substrate temperature of 1085°C and NH_3 flow of 30 cm^3/min and 50 cm^3/min ($n_{edge} \sim 5 \times 10^{10}$ cm^{-2} and $n_{screw} = 5.5 \times 10^8$ cm^{-2}, estimated as in [22]). At that time, the minimal RMS roughness value was observed for the sample grown at the same growth temperature but at the higher ammonia flow of 100 cm^3/min which had $n_{edge} \sim 1.3 \times 10^{11}$ cm^{-2} and $n_{screw} \sim 3.2 \times 10^8$ cm^{-2}. Additionally, we grew a 1200 nm-thick AlN in the same conditions which had dislocation density $n_{edge} \sim 3.4 \times 10^{10}$ cm^{-2} and $n_{screw} \sim 4.9 \times 10^8$ cm^{-2}. Most likely, the ambiguity in determination of the optimal growth conditions is caused by a trade-off between dislocation density and surface morphology which explained by the fact that a higher nucleation density induces both larger dislocation density and smoother surface.[27]

3.2 Plasma-assisted MBE growth of AlN layer

In this work we also developed PA-MBE growth conditions for AlN templates on sapphire substrates. A 80 nm-thick nucleation AlN layer was grown at temperature of 740°C using a migration enhanced epitaxy (MEE) mode with alternating switch of aluminium (Al) and nitrogen plasma (N*) flows[28-30] as shown by diagram in Fig. 3(a). Flows intensities and switching durations in this mode were determined on conditions that provide an excess of metal atoms on the surface during Al-open stage and a nitrogen dose supplied during N*-open stage sufficient for suppression of Al droplets' formation; these parameters are given in Fig. 3(a) too. After the nucleation layer, a 740 nm thick AlN in metal-modulated epitaxy (MME) mode[31] was grown followed by a 320 nm thick AlN grown at a continuous slightly metal-rich condition at the same temperature. During the growth of MME layer N* flow was kept constant whereas Al flow was periodically switched (2 min turn-on period, 0.5 min turn-off period) to prevent formation of Al droplets. AFM measurement revealed RMS roughness of ~0.9 nm for the layer which is comparable with our best AlN layer grown by ammonia-MBE. Dislocation density values for the PA-MBE AlN layer were $n_{edge} \sim 3.4 \times 10^{10}$ cm^{-2} and $n_{screw} \sim 3.3 \times 10^{9}$ cm^{-2}. The screw dislocation density in this sample is about by one order higher in comparison with the thick AlN grown by ammonia-MBE in step-flow mode.

3.3 Growth of HEMT heterostructures and their 2DEG properties

The obtained results on optimisation of NH_3-MBE of AlN layers demonstrating the trade-off between dislocation density and surface roughness make it difficult to select the optimal growth condition for HEMT heterostructures because of big importance of both structural quality and interfaces smoothness to provide good 2DEG properties.[32, 33] In our case, when comparing different AlN layers grown at higher temperatures (T = 1085°C and 1190°C) which demonstrated the best structural properties and surface roughness, we accepted the T = 1085°C and NH_3 flow of 100 cm^3/min as the optimal conditions. The layers with a lower dislocation density had a higher (by a factor of 3.5 or even more) RMS roughness. In our assumption, using of the substantially rougher templates for HEMT heterostructures would worsen 2DEG mobility.

Using the accepted optimised growth condition for nucleation and buffer AlN, two HEMT heterostructures differing by just 80 nm-thick nucleation layer were grown in two separate runs (schematic design is shown in Fig. 4). While the AlN nucleation layer of the first

structure was grown in the optimal NH_3-MBE conditions (T = 1085°C, 100 cm^3/min NH_3 flow), nucleation layer for the second one was grown by PA-MBE in MEE mode (the same conditions as shown in Fig. 3(a)). All the subsequent layers in the heterostructures were grown in the identical conditions by ammonia-MBE only. The buffer structure consisted of AlN, $Al_{0.3}Ga_{0.7}N$ and $Al_{0.09}Ga_{0.91}N$ separated by gradient-composition AlGaN layers as shown in Fig. 4. The active GaN layer had a relatively small thickness of 200 nm to prevent a creation of parasitic conductive channels. The $Al_{0.3}Ga_{0.7}N$ barrier layer included a Si-doped interlayer to provide a sufficiently high 2DEG density. The 800 nm-thick AlN buffer layer was grown at the same optimal ammonia-MBE conditions (T = 1085°C, 100 cm^3/min NH_3 flow) for both heterostructures. The optimum temperature for AlGaN and GaN layers was determined separately. For that, a GaN growth rate was determined as a function of substrate temperature keeping the constant NH_3 flow of 100 cm^3/min. An increase of GaN growth temperature results in a higher crystal quality because of enhancement of adatom mobility and formation of larger grains. On the other hand, when a growth temperature exceeds the critical value corresponding to GaN decomposition, a surface roughness increases leading to a drastic decrease of electron mobility. Therefore, the optimum GaN growth temperature can be determined as a threshold value corresponding to the beginning of GaN thermal decomposition.[34-36] In our experiment for the used NH_3 flow of 100 cm^3/min the value was determined to be 945°C. The same growth temperature and NH_3 flow values were used for growth of buffer AlGaN as well as barrier layers.

AFM scans of the grown HEMT surfaces are shown in Fig. 5 together with RMS roughness values σ. The scans demonstrate similar morphologies without of any terraces. Therefore, the higher roughness of the HEMT heterostructures (σ = 2.5 - 3 nm) in comparison with AlN templates (σ = 0.7 - 0.9 nm) can be attributed to contribution from AlGaN and GaN layers.

Both the grown HEMT heterostructures demonstrated rather good 2DEG properties (Fig. 6) in comparison with our previous results obtained for heterostructures grown at lower NH_3 flow and AlN growth temperature.[37] A slightly higher 2DEG mobility of about 2000 $cm^2/(V \cdot s)$ at 2DEG density of 1.17×10^{13} cm^{-2} was achieved for the heterostructure grown by combined MBE (PA nucleation and NH_3-MBE the rest layers) despite of the larger measured RMS surface roughness. Taking into account the observed inhomogeneity of 2DEG properties (Fig. 6), one should interpret the slightly higher 2DEG mobility of the combined MBE sample as a run-to-run variation of growth conditions rather than any specific effect of the PA MEE nucleation AlN. The obtained results demonstrate a possibility of successful combination of different epitaxy approaches within a single growth process,

which will contribute to development of new type of hybrid epitaxy uniting advantages of several technologies.

4. Conclusions

We performed optimisation of NH_3-MBE growth conditions of AlN templates on sapphire substrates using XRD and AFM measurements. The minimal surface roughness of ~0.7 nm was achieved for the 320 nm-thick AlN layer grown at substrate temperature of 1085°C and NH_3 flow of 100 cm^3/min and demonstrating a terrace-like surface morphology. In addition, PA mode was applied to growth AlN template including a MEE nucleation layer and demonstrating a similar surface roughness of ~0.9 nm. The optimised epitaxy modes of AlN nucleation layer (NH_3-MBE and PA-MBE, respectively) were used to grow two otherwise nominally identical HEMT heterostructures by NH_3-MBE which demonstrated relatively good 2DEG properties. A slightly better 2DEG performances (mobility of about 2000 $cm^2/(V \cdot s)$ at density of 1.17×10^{13} cm^{-2}) were measured for the combined MBE HEMT structure which is likely caused by a run-to-run variation of growth conditions. The results demonstrate a possibility of successful combination of different epitaxy technologies within a single growth process.

Acknowledgments

This work was supported in part by State programs of scientific research of Belarus "Photonics, opto- and microelectronics" 2.1.01, 2.1.04 and Union State Scientific Program 5.3 Luch (Contract #618).

References

1) U. K.Mishra, P. Parikh, and Y. F. Wu, Proc. IEEE **90** 1022 (2002).
2) B. Zou, H. Liang, and K. M. Lau, Phys. Status Solidi C **7** 2171 (2010).
3) D. Christy, A. Watanabe, and T. Egawa, AIP Adv. **4** 107104 (2014).
4) B. J. Baliga, Semicond. Sci. Technol. **28** 074011 (2013).
5) S. Sano, K. Ebihara, T. Yamamoto, T. Sato, and N. Miyazava, SEI Tech. Rev. **86** 65 (2018).
6) F. Medjdoub, M. Zegaoui, N. Waldhoff, B. Grimbert, N. Rolland, and P.-A. Rolland, Appl. Phys. Express **4** 064106 (2011).
7) D. C. Sheridan, D. Y. Lee, A. Ritenour, V. Bondarenko, J. Yang, and C. Coleman, Proc. PCIM Europe 2014, 2014, p. 1-7.
8) Y. Tang, K. Shinohara, D. Regan, A. Corrion, D. Brown, J. Wong, A. Schmitz, H. Fung, S. Kim, and M. Micovic, IEEE Electron Device Lett. **36** [6] 549 (2015).
9) U. Forsberg, A. Lundskog, A. Kakanakova-Georgieva, R.Ciechonski, and E. Janzén, J. of Cryst. Growth **311** [10] 3007 (2009).
10) J. Cheng, X. Yang, L. Sang, L. Guo, J. Zhang, J. Wang, C. He, L. Zhang, M. Wang, F. Xu, N. Tang, Z. Qin, X. Wang, and B. Shen, Sci. Rep. **6** 23020 (2016).
11) A. A. Arendarenko, V. A. Oreshkin, Yu. N. Sveshnikov, I. N. Tsyplenkov, Modern Electronic Materials **2** 33 (2016).
12) E. Ahmadi, S. Keller, and U. K. Mishra, J. Appl. Phys. **120** 115302 (2016).
13) G. Steinhoff, M. Hermann, W. J. Schaff, L. F. Eastman, M. Stutzmann, M. Eickhoff, Appl. Phys. Lett. **83** 177 (2003).
14) H. H. Lee, M. Bae, S. H. Jo, J. K. Shin, D. H. Son, C. H. Won, J. H. Lee, Sens. Actuator B-Chem. **234** 316 (2016).
15) M. S. Z. Abidin, A. M. Hashim, M. E. Sharifabad, S. F. A. Rahman, T. Sadoh, Sensors **11** 3067 (2011).
16) J. R. Heffelfinger, D. L. Medlin, K. F. McCarty, J. Appl. Phys. **85** 466 (1999).
17) R. Banal, M. Funato, Y. Kawakami, Appl. Phys. Lett. **92** 241905 (2008).
18) F. Chaumeton, S. Gauthier, D. Martrou, AIP Adv. **5** 067108 (2015).
19) J. Jasinski, Z. Liliental-Weber, Q. S. Paduano, D. W. Weyburne, Appl. Phys. Lett. **83**, 2811 (2003).
20) S. Tamariz, D. Martin, N. Grandjean, J. of Cryst. Growth **476** 58 (2017).
21) S. Nikishin, B. Borisov, M. Pandikunta, R. Dahal, J. Y. Lin, H. X. Jiang, H. Harris, M.

Holtz, Appl. Phys. Lett. 95, 054101 (2009).

22) J. Xiong, J. Tang, T. Liang, Y. Wang, C. Xue, W. Shi, W. Zhang, Appl. Surf. Sci. **257** 1161 (2010).

23) M. A. Moram, M. E. Vickers, Rep. Prog. Phys.**72** 036502 (2009).

24) A. N. Alexeev, D. M. Krasovitsky, S. I. Petrov, V. P. Chaly, V. V. Mamaev, V. G. Sidorov, Semiconductors **49** 92 (2015).

25) D. A. Neumayer, J. G. Ekerdt, Chem. Mater. **8** 9 (1996).

26) F. Brunner, H. Protzmann, M. Heuken, A. Knauer, M. Weyers, M. Kneissl, Phys. Status Solidi C **5** 1799 (2008).

27) M. Ishida, T. Hashimoto, T. Takayama, Imafuji, M. Yuri, A. Yoshikawa, K. Itoh, Y. Terakoshi, T. Sugino, J. Shirafuji, Mat. Res. Soc. Symp. Proc. **468** 69 (1997).

28) Y. Horikoshi, M. Kawashima, H. Yamaguchi, Jpn. J. Appl. Phys. **25** L868 (1986).

29) D. V. Nechaev, P. A. Aseev, V. N. Jmerik, P. N. Brunkov, Y. V. Kuznetsova, A. A. Sitnikova, V. V. Ratnikov, S. V. Ivanov, J. of Cryst. Growth **378** 319 (2013).

30) V. N. Jmerik, D. V. Nechaev, S. Rouvimov, V. V. Ratnikov, P. S. Kop'ev, M. V. Rzheutski, E. V. Lutsenko, G. P. Yablonskii, M. Aljohenii, A. Aljerwii, A. Alyamani, S. V. Ivanov, J. Mater. Res. **30** 2871 (2015).

31) D. V. Nechaev, P. N. Brunkov, S. I. Troshkov, V. N. Jmerik, S. V. Ivanov, J. of Cryst. Growth **425** 9 (2015).

32) E. Ahmadi, S. Keller, U. K. Mishra, J. Appl. Phys. **120** 115302 (2016).

33) F. Alessio Marino, N. Faralli, T. Palacios, D. K. Ferry, S. M. Goodnick, M. Saraniti, IEEE Trans. Electron Devices **57** 353 (2010).

34) J. B. Webb, H. Tang, J.A. Bardwell, S. Moisa, C. Peters, T. MacElwee, J. of Cryst. Growth **230** 584 (2001).

35) J. B. Webb, H. Tang, J. A. Bardwell, Y. Liu, J. Lapointe, T. MacElwee, Phys. Status Solidi A **194** 439 (2002).

36) A.N. Alexeev, B.A. Borisov, V.P. Chaly, D.M. Demidov, A.L. Dudin, D.M. Krasovitsky, Yu.V. Pogorelsky, A.P. Shkurko, I.A. Sokolov, M.V. Stepanov, A.L. Ter-Martirosyan, Mater. Res. Soc. Internet Journal of Nitride Semiconductor Research **4** e6 (1999).

37) E. V. Lutsenko, M. V. Rzheutski, A. G. Vainilovich, I.E. Svitsiankou, N. P. Tarasuk, G. P. Yablonskii, A. Alyamani, S. I. Petrov, V. V. Mamaev, A. N. Alexeev, Phys. Status Solidi A **215** 1700602 (2018)

Figure Captions

Fig. 1. SEM images (1 μm × 1 μm) of 0.28 μm thick AlN epilayers grown at different NH_3 flows and substrate temperatures (σ denotes RMS surface roughness values obtained from AFM of the same samples).

Fig. 2. Growth temperature dependences of the FWHM of the XRD rocking curves measured for 002 and 101 AlN diffraction peaks in symmetric and skew symmetric configurations, respectively.

Fig. 3. (a) Diagram demonstrating growth conditions of nucleation AlN layer by MEE and (b) 5 μm × 5 μm AFM scan of the AlN layer grown by PA-MBE.

Fig. 4. Schematic design of the HEMT heterostructures.

Fig. 5. 5 μm × 5 μm AFM scan of the HEMT heterostructures grown by (a) fully ammonia and (b) combined MBE.

Fig. 6. 2DEG properties of the grown HEMT heterostructures (the solid lines are isoresistance curves corresponding to different sheet resistance values).

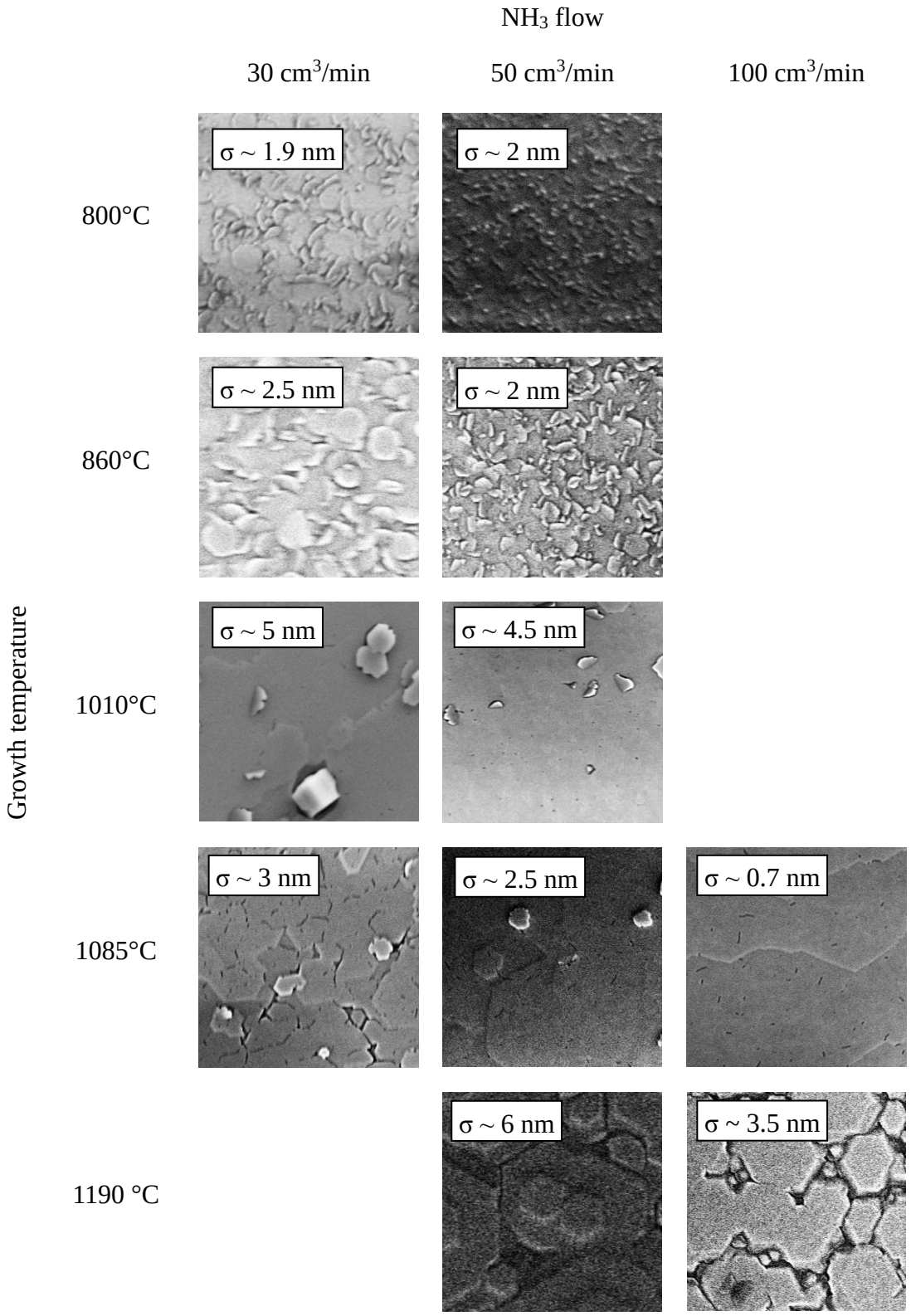
NH3 flow
30 cm3/min
50 cm3/min
100 cm3/min
Growth temperature
800°C
860°C
1010°C
1085°C
1190 °C
σ ~ 1.9 nm
σ ~ 2 nm
σ ~ 2.5 nm
σ ~ 2 nm
σ ~ 5 nm
σ ~ 4.5 nm
σ ~ 3 nm
σ ~ 2.5 nm
σ ~ 0.7 nm
σ ~ 6 nm
σ ~ 3.5 nm

Fig.1.

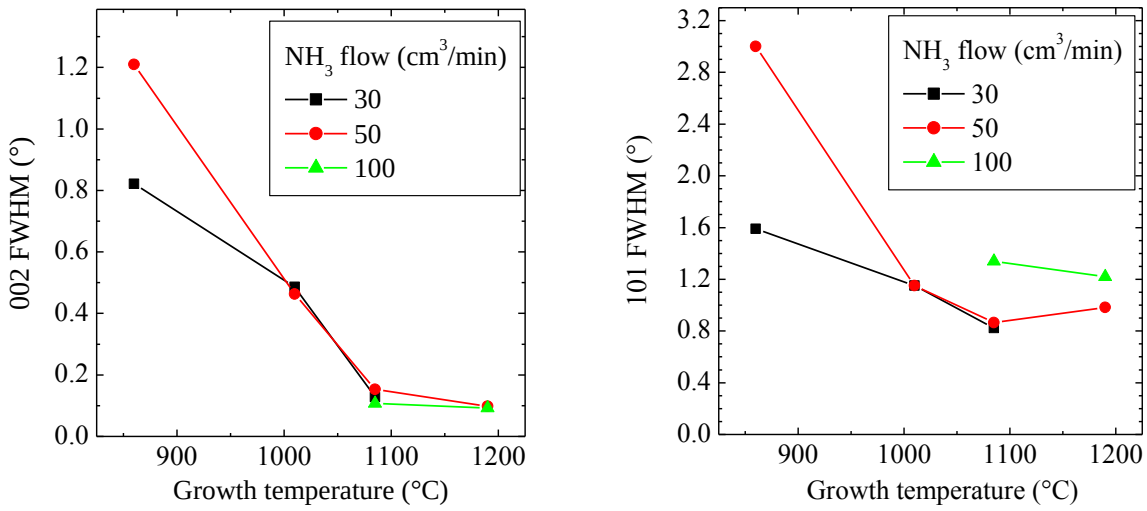
002 FWHM (°)
101 FWHM (°)
Growth temperature (°C)
NH3 flow (cm3/min)
30
50
100

Fig. 2.

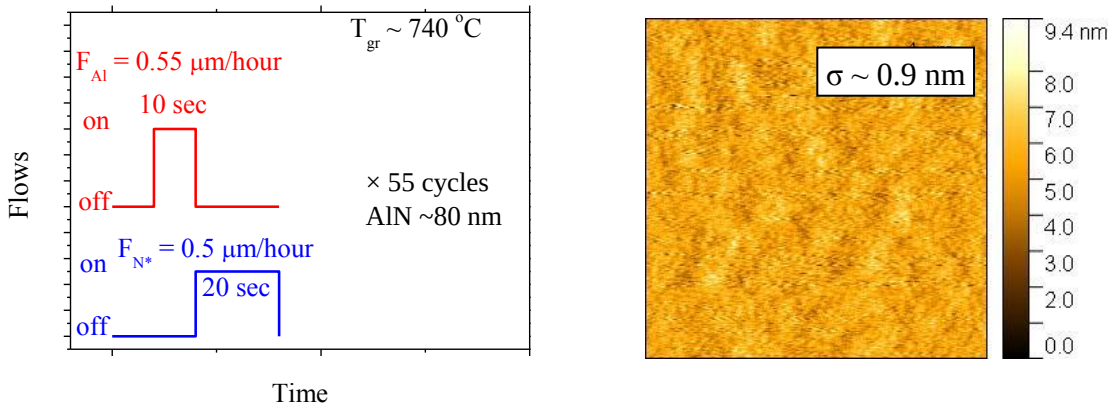
T gr ~ 740 °C
F Al = 0.55 µm/hour
10 sec
on
off
× 55 cycles
AlN ~80 nm
on
F N* = 0.5 µm/hour
20 sec
off
Flows
Time
σ ~ 0.9 nm
9.4 nm
8.0
7.0
6.0
5.0
4.0
3.0
2.0
0.0

(a) (b)

Fig. 3.

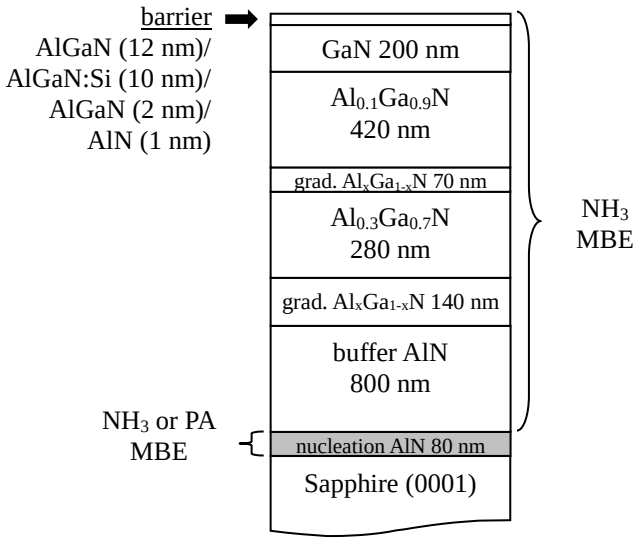
barrier
AlGaN (12 nm)/
AlGaN:Si (10 nm)/
AlGaN (2 nm)/
AlN (1 nm)
GaN 200 nm
Al0.1Ga0.9N
420 nm
grad. AlxGa1-xN 70 nm
Al0.3Ga0.7N
280 nm
grad. AlxGa1-xN 140 nm
buffer AlN
800 nm
NH3
MBE
NH3 or PA
MBE
nucleation AlN 80 nm
Sapphire (0001)

Fig. 4.

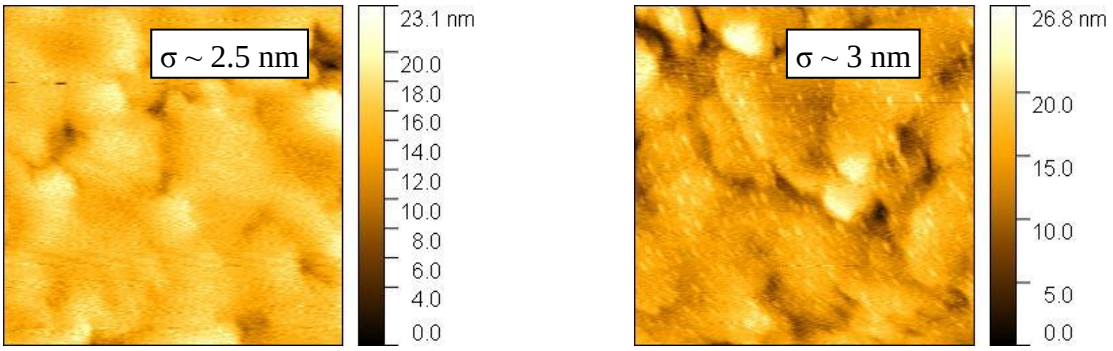
σ ~ 2.5 nm
23.1 nm
20.0
18.0
16.0
14.0
12.0
10.0
8.0
6.0
4.0
0.0
σ ~ 3 nm
26.8 nm
20.0
15.0
10.0
5.0
0.0

(a) (b)

Fig. 5.

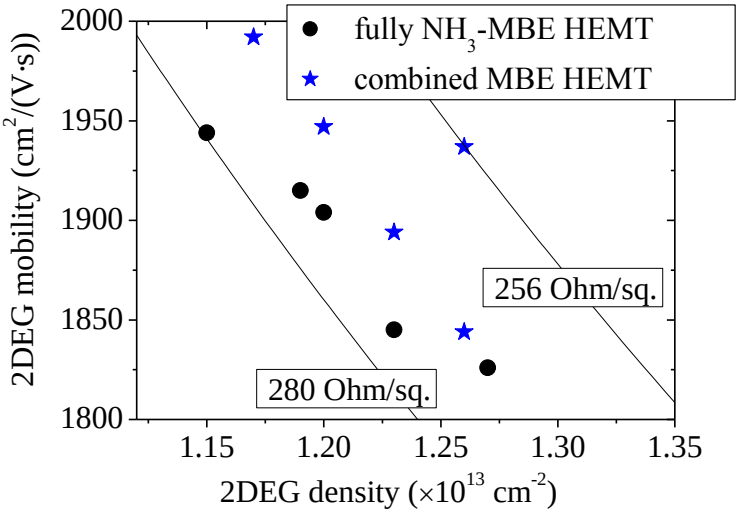
fully NH3-MBE HEMT
combined MBE HEMT
256 Ohm/sq.
280 Ohm/sq.
2DEG mobility (cm2/(V·s))
2DEG density (×10^13 cm^-2)
2000
1950
1900
1850
1800
1.15
1.20
1.25
1.30
1.35

Fig. 6.